Rockefeller University

COO-2232A-27

Conf.-750855--9

EUROPEAN ORGANIZATION FOR NUCLEAR RESEARCH

High Transverse Momentum Phenomena Involving π and η Mesons at the CERN ISR

F.W. Büsser*), L. Camilleri, L. Di Lella,
B.G. Pope and A.M. Smith
CERN, Geneva, Switzerland

B.J. Blumenfeld and S.N. White
Columbia University, New York, U.S.A.**)

A.F. Rothenberg, S.L. Segler and M.J. Tannenbaum
The Rockefeller University, New York, U.S.A.***)

M. Banner, J.B. Chèze, H. Kasha§), J.P. Pansart, G. Smadja,
J. Teiger, H. Zaccone and A. Zylberstejn
CEN, Saclay, France

ABSTRACT

The inclusive production of π and η mesons at $\theta_{CM} = 90^\circ$ has been measured for proton-proton collisions at five centre-of-mass energies between 23.5 GeV and 62.4 GeV. The momentum correlation of charged particles emitted together with a large transverse momentum π has also been studied using two magnetic spectrometers each centred at $\theta_{CM} = 90^\circ$.

Submitted to the International Symposium on Lepton and Photon Interactions at High Energies

Stanford University, 21 -27 August 1975

---

*) Permanent address, II Institut für Experimentalphysik, Hamburg, BDR.

**) Research supported in part by the NSF.

***) Research supported in part by the AEC.

§) Permanent address, Yale University, New Haven Conn., U.S.A.

DISCLAIMER

I. Apparatus.

The experimental apparatus shown in Fig. 1 and described in detail elsewhere [1,2], was located around 90° on opposite sides of an interaction region. The charged particles were detected and analysed in two magnetic spectrometers. Each spectrometer was equipped with a gas Čerenkov counter located in the magnet. The Čerenkov in arm 1, filled with isobutane at atmospheric pressure, had a momentum threshold for pion detection of 2.8 GeV/c in the laboratory system. The Čerenkov in arm 2 was not used in this analysis.

Photons from the decay of high momentum π^0 and η mesons were identified in arm 2 by their electromagnetic showers in the total absorption lead-glass Čerenkov counter array located behind the arm 2 spectrometer. This array consisted of 119 blocks, arranged in 7 horizontal rows of 17 blocks. Each block was 35 cm thick, corresponding to 14.8 radiation lengths, and had a cross-section of 15 x 15 cm^2. The distance between the centre of the intersection region and the front wall of the array was 3.48 m.

The high momentum charged pions were measured in arm 1. The angular apertures of the detectors are listed in Table 1.

Four 1 m^2 scintillation counters, B_1 to B_4, not shown in Fig. 1, were also used. Counters B_1 and B_2 were centred on the downstream vacuum pipe of Ring 1, while B_3 and B_4 were similarly centred on Ring 2. Counters B_1 and B_4 were located at a distance of 5.65 m from the crossing point, while B_2 and B_3 were at 4.65 m. The coincidences B_1B_4 and B_2B_3 were timed to select an almost pure sample of beam-beam collisions.

II. Triggers.

a) π^0 and η .

The apparatus was triggered whenever sufficient energy to exceed a set electronic threshold was deposited in any 2 x 2 block

square of the lead-glass array. However, to ensure that the event originated from a beam-beam collision, the energy requirement was put into coincidence with any of the following three signals : BB $\equiv B_1B_4$ or B_2B_3; a coincidence between the H_1 and H_2 hodoscopes; a coincidence between the H_1' and H_2' hodoscopes. The trigger was thus not fully inclusive for γ -rays but resulted in a triggering bias which is described below. During data taking, the electronic threshold was adjusted as a function of the ISR luminosity in order to keep the triggering rate at a level of around 2 sec^{-1}. Threshold values ranging between 1.0 and 2.4 GeV were used.

b) $\pi^{\pm}$

This trigger required a coincidence between the signals coming from the three hodoscopes H_1, H_2, H_3 and from the gas Čerenkov counter C. This last requirement selected events containing an electron within the apparatus as well as those events with high momentum pions. To help reject events with low energy electrons a signal from hodoscope H_5 located behind 5.5 radiation lengths of material was also required. This trigger was fully inclusive.

For each trigger, digitized information from the apparatus was written on to magnetic tape, as described in Ref. 2. Details of the calibration and monitoring of the lead-glass counters are given elsewhere [3].

III. Single Particle Analysis.

The data analysis was different for charged and neutral pions.

Charged pions.

The Čerenkov requirement in the trigger produced a sample of events containing either an electron or a pion of momentum greater than 2.8 GeV/c. This threshold corresponds to a centre-of-mass momentum of 3.16 GeV/c. In order to avoid difficulties in

analysing events near the pion threshold where the detection efficiency of the Cerenkov varied very rapidly with momentum, only events with transverse momenta in the centre-of-mass greater than 3.3 GeV/c were accepted. In addition, geometrical cuts were applied in order to eliminate badly reconstructed tracks which might simulate high p_T events.

The momentum resolution of the magnet is given by $\Delta p/p = \sqrt{(.025)^2 + (.02p)^2}$ where p is in GeV/c. This resolution was taken into account to correct the measured transverse momentum spectrum.

The background to the charged pions was assumed to be negligible.

Neutral mesons.

The data were analysed by searching the recorded events for energy clusters in the lead-glass array. An energy cluster was defined as a group of no more than seven adjacent blocks, with at least 300 MeV deposited in a single block and the others having pulse heights corresponding to at least 20 MeV. In addition, the cluster was constrained to be no more than four blocks wide or high, and to be centred at a point at least 15 cm from the edge of the array. These criteria were empirically determined to reject background clusters not originating from beam-beam collisions. Furthermore, if a charged particle were incident on the lead-glass array at a distance less than 18 cm away from the cluster centre, the cluster was rejected.

Events without a BB signal were considered only if at least one track originating from the interaction diamond could be reconstructed in either arm from the spark chambers preceding the magnet.

For events containing two clusters, each cluster was interpreted as being due to a single photon, and the invariant mass, $M_{\gamma\gamma}$, of the photon pair was calculated. The directions of the

photons were obtained by connecting the centres of the two clusters with the interaction vertex. The vertex was directly obtained if reconstructed tracks were present in the event. It was assumed to be the centre of the interaction diamond, for events with no tracks. Reconstructed tracks were present in approximately 20% of the events at each value of $\sqrt{s}$.

Fig. 2 shows the number of two cluster events as a function of $M_{\gamma\gamma}$ for four values of $\sqrt{s}$. These four distributions are very similar in form and each has two peaks, the first occuring at $M_{\gamma\gamma} = M_{\pi^0}$. The background under the second peak is in each case estimated by an exponential interpolation as shown by the dashed lines. This second peak with background subtracted occurs at $M_{\gamma\gamma}$ = 540 MeV. This value and the width of the peak are consistant with the η meson, when the uncertainties in the opening angle measurement and in the absolute energy calibration are taken into account.

It must be stressed that the π^0 mesons contributing to the distribution of Fig. 2 have an average momentum much lower than that of the η mesons. This is due to the fact that the two photons from the decay $\pi^0 \to \gamma\gamma$ will in general overlap in a single cluster for π^0 momenta above $\sim$ 2.5 GeV/c. On the other hand, in the decay $\eta \to \gamma\gamma$ the two clusters are distinct for momenta up to $\sim$9 GeV/c, while below 2.5 GeV/c, the probability that both photons enter the lead-glass array is small, owing to their large opening angle ($\gtrsim 25^\circ$).

Another consequence of the above facts is that the events containing one cluster only, with energy above 2.5 GeV, are mainly due to π^0's of the same energy. Clusters resulting from only one of the photons from η decay would require, in fact, a parent with an energy higher than that of the cluster. Such events are suppressed by approximately one order of magnitude, owing to the steep fall of the production cross-section with

increasing energy of the meson.

Two cluster events were accepted as candidates for the decay $\eta \to \gamma\gamma$, if $M_{\gamma\gamma}$ was between 450 and 650 MeV. The background under the peak, estimated as described above, was studied for momentum dependence at $\sqrt{s}$ = 52.7 GeV where the data had the best statistics. The events were divided into two η momentum intervals containing approximately the same number of events. For the first interval, $3 \leq p_\eta < 4$ GeV/c, this background amounted to (55 ± 5)% of all $\eta \to \gamma\gamma$ candidates. It was (58 ± 5)% in the second interval, $4 \leq p_\eta < 6$ GeV/c. Since these values were equal within errors, it was inferred that the background under the peak was independent of the η momentum above 3 GeV/c. The backgrounds at the other centre-of-mass energies were assumed to behave similarly, and the resulting signal to background ratios are listed in Table 2, where the errors are statistical only.

Two-cluster events with $M_{\gamma\gamma}$ between 100 and 200 MeV, as well as all one-cluster events, were accepted as candidates for the decay $\pi^\circ \to \gamma\gamma$.

For both $\pi^\circ \to \gamma\gamma$ and $\eta \to \gamma\gamma$ decays, the solid angle and detection efficiency was calculated using a Monte Carlo program. The overall acceptance for the decay $\eta \to \gamma\gamma$ was found to be a steep function of the η momentum, increasing by a factor of 5 between 3 and 4.5 GeV/c.

In order to determine the inclusive cross-section from the data, it was necessary to know the triggering bias mentioned above. This bias was deduced at each value of $\sqrt{s}$, by dividing the events into four categories, I) events accompanied by the BB signal and at least one track; II) events accompanied by the BB signal only; III) events without the BB signal but accompanied by at least one track; and IV) events with neither the BB signal nor any track. The events belonging to category IV were not detected, of course, because of the triggering bias. Their

number was estimated assuming, as in Ref. 4, that the ratio of the number of events of category I to that of category II is equal to the ratio of the number of events of category III to that of category IV. Under this assumption, the events undetected because of the triggering bias were estimated at each $\sqrt{s}$ value and the correction factor was found to be independent of momentum for π^0's. It was assumed to be the same for η's and π^0's. This latter assumption was checked at $\sqrt{s}$ = 52.7 GeV where the trigger bias for η's was found to be within 1% of that for π^0's. The trigger bias (B), defined as the number by which the measured events have to be multiplied to obtain the inclusive yield, is listed in Table 2 for each value.

IV. Results on inclusive cross-sections.

Fig. 3 shows the invariant cross-sections for both π^0's and η's at $\sqrt{s}$ = 52.7 GeV, as a function of p_T^*, the meson transverse momentum in the centre-of-mass system. The errors shown are statistical. The branching ratio for the decay $\eta \to \gamma\gamma$ was taken to be 0.38.

The shape of the η production cross-section appears to be parallel, within statistics, to that of the π^0, in the p_T^* intervall between 3 and 5.6 GeV/c. Lack of statistics prevented the determination of the η differential cross-section at all values of $\sqrt{s}$ studied. However, by assuming in each case that the shape of the η distribution was the same as that of the π^0 distribution, the ratio η/π^0 was calculated by integrating the η and π^0 spectra over the interval $3.0 < p^* < 4.9$ GeV/c. The values obtained are given in Table 2 where the errors are statistical only.

In order to check the p_T^* dependence, the η/π^0 ratio was also determined for the more restricted p^* interval $4.0 < p^* < 4.9$ GeV/c and found to be in good agreement with the results from the larger p^* interval. It was thus concluded that the η/π^0 ratio

is independent of p^* and $\sqrt{s}$ in the large p_T region, and equal to 0.55 ± 0.1 where the error includes an estimate for the uncertainties in the acceptance calculation.

Figs. 4a - c show the invariant cross-sections for charged and neutral pions as a function of p_T^* at three values of $\sqrt{s}$. From these it can be seen that there is general agreement between the charged and neutral cross-sections. The ratio π^+/π^- is found to be 1.2 but uncertainties in the relative normalizations prevent the absolute comparison of neutral with charged pions.

In order to study the s dependence, the invariant cross-sections for charged and neutral pions were fitted to the form

$$E \frac{d^3\sigma}{dp^3} = \frac{A}{p^n} e^{-bp_T/\sqrt{s}}$$

Neutral pion events with $p_T^* > 2.46$ GeV/c at all five values of $\sqrt{s}$ were used in the fit. For charged pions the p_T^* range started at 3.3 GeV/c and only data at $\sqrt{s}$ = 44.8, 52.7, and 62.4 GeV were used.

The values of A, b, and n obtained for π^+, π^- and π^0's are summarised in Table 3 where the errors are statistical only. The neutral pion fit is illustrated in Fig. 5. A fit to the charged averaged pion data $(\pi^+ + \pi^-)/2$ gave the following values : $A = (4.88 \pm 0.8) \times 10^{-27}$, $b = 30.8 \pm 1.7$ and $n = 7.8 \pm 0.2$. This may be compared with the result obtained on restricting the π^0 data to the same range of $\sqrt{s}$ and p_T^* : $A = (12.5 \pm 1.2) \times 10^{-27}$, $b = 26.2 \pm 1.0$ and $n = 8.4 \pm 0.1$.

The present π^0 results agree fairly well with the earlier data of Ref. 4 where a fit to the same function gave $A = (1.54 \pm 0.10) \times 10^{-26}$, $b = 26.10 \pm 0.50$ and $n = 8.24 \pm 0.05$. The error in the absolute normalization of the present experiment of $\pm$ 26% arising mainly from the uncertainty in the absolute

energy calibration ($\pm$ 3%), is thought to make the data more reliable than those of Ref. 4.

V. Results on Correlations.

In the course of measuring high transverse momentum mesons, the charged particles emitted within the acceptance of the apparatus coincidentally with the high momentum particle were also recorded. Data are presented for correlations with large p_T^* pions at four centre-of-mass energies, however insufficient data were available to make a useful study of the charged particles correlated with the observed η 's.

The momenta of the correlated charged particles were measured in the magnetic spectrometers and were always assumed to be pions. To be considered in the analysis, a charged particle had to traverse one counter in each of the three appropriate scintillation hodoscope planes setting the corresponding bits and have its track originate within the interaction diamond. The high p_T^* π^0 was always detected in arm 2 of the apparatus and this made it convenient to consider separately the correlation with charged particles in arm 1 and arm 2 which were separated in azimuthal angle ϕ, by 180°.

The high p_T^* charged pions were detected in arm 1 and due to the limited solid angle in this arm, only the correlations with charged particles in the opposite arm will be presented.

A function F was defined as

$$F = \frac{\int_{\Delta y_1 \Delta \phi_1} dy_1 d\phi_1 \int_{p_1}^{\infty} dp_{T'} \int_{\Delta \phi_2} \frac{d^6\sigma}{dy_1 d\phi_1 dp_{T'} dy_2 d\phi_2 dp_{T2}} d\phi_2}{\int_{\Delta y_1 \Delta \phi_1} dy_1 d\phi_1 \int_{p_1}^{\infty} dp_{T'} \frac{d^3\sigma}{dy_1 d\phi_1 dp_{T'}}}$$

This is the probability, per interaction yielding a pion of $p_T > p_1$ within the detector, of observing a particle of momentum p_{T2} and rapidity y_2 within the ϕ acceptance of the apparatus.

This function was determined for those interactions in which a π^0 of $p_T^* > 3$ GeV/c was measured in arm 2, and is presented in Figs. 6 and 7 for the cases in which the charged particles are emitted with $\Delta\phi \approx 0^\circ$ and $\Delta\phi \approx 180^\circ$ respectively.

For comparison with low momentum behaviour, the function F was also studied using a fully inclusive trigger for charged particles within the acceptance of the apparatus. The triggers employed were a coincidence between the hodoscopes in arm 1, $H_1\ H_2\ H_3$ or between those in arm 2, $H_1'\ H_2'\ H_3'$. These triggers gave no bias for detecting charged particles in either arm.

In this case F is the probability, per inelastic interaction, of yielding a particle of $p_T = p_2$ and $y = y_2$ within the ϕ acceptance of the apparatus. It is of course the same for both arms of the detector and was found to be independent of $\sqrt{s}$. It is shown in Figs. 6 and 7 for comparison with the high momentum data.

When the charged particles are emitted with $\Delta\phi \approx 180^\circ$ from the high momentum π^0 (Fig. 7), F is found to be independent of s but at least an order of magnitude larger than the probability for the fully inclusive trigger for charged particles with $p_T^* > 1$ GeV/c. This is illustrated more clearly in Fig. 8 where F is presented as a function of s for three momentum bands of the coincident charged particle.

Different behaviour is observed for F when the charged particles are emitted close in ϕ to the high transverse momentum π^0 (Fig. 6). In this case F increases appreciably with s as can be seen more clearly in Fig. 9. It should be noted that all the correlation measurements in association with the π^0's involves a small inefficiency due to the rejection of those events mentioned earlier in which a charged particle was incident on the lead-glass

less than 18 cm from the centre of the π^o energy cluster. This inefficiency could not greatly effect the results presented since the magnetic field would normally separate from the π^o any charged particle emitted close to its direction.

The function F observed in interactions in which a charged pion of $p_T^* > 3.3$ GeV/c was produced are presented in Figs. 10a - c for the correlated particle being emitted with $\Delta\phi \approx 180^o$ at three values of $\sqrt{s}$. For comparison the corresponding quantities for neutral pion correlations with $\Delta\phi \approx 180^o$ and with $\Delta\phi \approx 0^o$ are also shown in these Figures. Whether the high p_T pion is neutral or charged does not seem to affect the behaviour of the $\Delta\phi = 180^o$ probability F. The charged meson correlations were examined more closely by considering separately the correlations for π^+ and π^- mesons with particles of the same and opposite charges. The results are presented in Fig. 11 again in terms of F. Identical behaviour is observed for all charge combinations at $\sqrt{s} \approx 50$ GeV.

The momentum dependence of the results is consistent with the data of Ref. 5 on correlations between high transverse momentum π^o's. The opposite sides correlations ($\Delta\phi \approx 180^o$) can be explained in terms of momentum conservation which predicts an increase of F with p_T.

The same sides correlations however, can not be explained by momentum conservation. Here F also increases with p_T with respect to its behaviour for the inclusive trigger and an explanation of this requires some dynamical effects to be present. The increase of the correlation with s may imply some phase space limitation. To examine whether the same sides correlation could be due to resonance production, the invariant mass spectrum for the high p_T π^o with the correlated charged particle was calculated, under the assumption that the charged particles were all π's. No structure was observed in this mass spectrum which

is shown in Fig. 12 for $\sqrt{s} \approx 50$ GeV. The mass resolution was estimated from a Monte Carlo calculation to be $\pm$ 60 MeV and approximately constant between 700 MeV and 1.5 GeV.

Acknowledgements

We wish to thank Professors R.L. Cool and L.M. Lederman for their interest and support; Messrs. M. Lemoine and G. Sicher for invaluable technical help; Miss M.A. Huber for assistance in the data analysis; and the ISR crew for the excellent performance of the machine.

REFERENCES

1) M. Banner et al., Phys. Letters 44B,573 (1973).

2) F.W. Büsser et al., Phys. Letters 53B,212 (1974).

3) J.S. Beale et al., Nuclear Instr. Methods 117,501 (1974).

4) F.W. Büsser et al., Phys. Letters 46B,471 (1973).

5) F.W. Büsser et al., Phys. Letters 51B,311 (1974).

Table 1

Angular apertures for the spectrometers
in the centre-of-mass system

	Particle type	θ^* degrees	ϕ^* degrees
ARM 1	$\pi^{\pm}$	90 ± 13	180 ± 5
ARM 2	$\pi^{\pm}$	90 ± 28	0 ± 8
ARM 2	π^{0}	90 ± 20	0 ± 7

Table 2

$\sqrt{s}$ GeV	η signal / background	Bias B	η/π^0 ratio
23.5	-	$1.973 \pm .107$	≤ 1.73
30.6	$.70 \pm .13$	$1.545 \pm .018$	$.42 \pm .08$
44.8	$.74 \pm .06$	$1.191 \pm .004$	$.56 \pm .04$
52.7	$.73 \pm .10$	$1.123 \pm .004$	$.58 \pm .05$
62.4	$.62 \pm .07$	$1.080 \pm .003$	$.55 \pm .06$

Table 3

Fitted parameters for the pion inclusive cross-sections

	π^+	π^-	π^0
A x 10^{27}	3.60 ± 0.66	5.19 ± 1.62	14.8 ± 0.6
b	30.8 ± 2.3	32.2 ± 2.4	25.2 ± 0.4
n	7.5 ± 0.17	7.86 ± 0.30	8.62 ± 0.04
χ^2/D.F.	72/63	70/64	261.5/178

Figure captions

Fig. 1 : Plan view of the experimental apparatus.

Fig. 2 : Invariant mass distributions of two photon events at four centre-of-mass energies.

Fig. 3 : Invariant cross-section for inclusive production of π^0's (Fig. 3a) and η's (Fig.3b) at $\theta_{cm} = 90^\circ$ and $\sqrt{s} = 52.7$ GeV. The curves shown in Figs. 3a and 3b are the best fits to the results of Ref. 4 multiplied by 0.72 and 0.40, respectively.

Fig. 4 : Invariant cross-section for the production of π^+, π^- and π^0 at $\theta_{cm} = 90^\circ$ and $\sqrt{s} = 44.8$ GeV (Fig. 4a), 52.7 GeV (Fig. 4b) and 62.4 GeV (Fig.4c).

Fig. 5 : The function $A\,(p_T/\sqrt{s}) = p_T^n\, E\, d^3\sigma/dp^3$, as deduced from the π^0 measurements using the best fit value $n = 8.62$. The errors are statistical only.

Fig. 6 : The function F, defined in the text, plotted as a function of p_T of the charged particles emitted close in azimuth ($\Delta\phi \approx 0^\circ$) to a π^0 with $p_T > 3$ GeV/c, for four values of $\sqrt{s}$. The probability per inelastic interaction is also shown.

Fig. 7 : The function F, plotted as a function of p_T of the charged particles emitted opposite in azimuth ($\Delta\phi \approx 180^\circ$) to a π^0 of $p_T > 3$ GeV/c.

Fig. 8 : The function F, plotted as a function of $\sqrt{s}$ for three p_T intervals for the charged particles emitted with $\Delta\phi \approx 180^\circ$ from a π^0 of $p_T > 3$ GeV/c.

Fig. 9 : The function F, plotted as a function of $\sqrt{s}$ for three p_T intervals for the charged particles emitted close in azimuth ($\Delta\phi \approx 0^\circ$) to a π^0 of $p_T > 3$ GeV/c.

Fig. 10 : The function F, plotted as a function of p_T of the charged particles emitted opposite in azimuth ($\Delta\phi \approx 180^\circ$) to a charged pion of $p_T > 3.3$ GeV/c at: 10a) $\sqrt{s}$ = 44.8 GeV; 10b) $\sqrt{s}$ = 52.7 GeV; 10c) $\sqrt{s}$ = 62.4 GeV. For comparison the corresponding results for charged particles emitted with azimuthal separations $\Delta\phi \approx 180^\circ$ and 0° from a π^0 of $p_T > 3$ GeV/c are also shown together with the fully inclusive result.

Fig. 11 : The function F (for π^+'s and π^-'s with $p_T > 3.3$ GeV/c) plotted as a function of p_T of the positively and negatively charged particles emitted opposite in azimuth to the high p_T pion at $\sqrt{s} \approx 50$ GeV.

Fig. 12 : The distribution in invariant mass, $M_{(\pi^0 \pi^\pm)}$ for charged pions emitted close in azimuth ($\Delta\phi \approx 0^\circ$) to a π^0 of $p_T > 3$ GeV/c.

PLAN VIEW OF APPARATUS

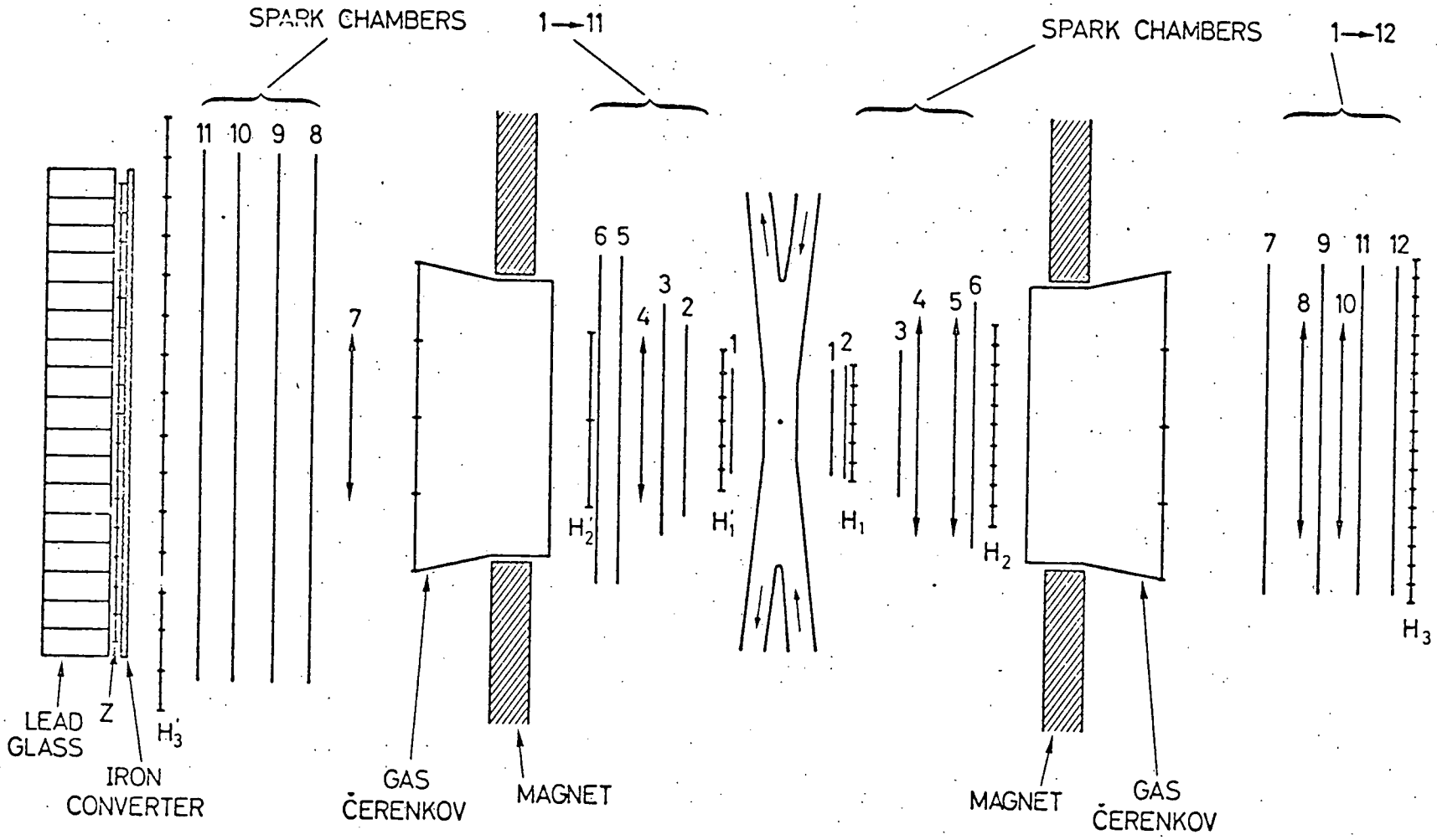

Fig. 1

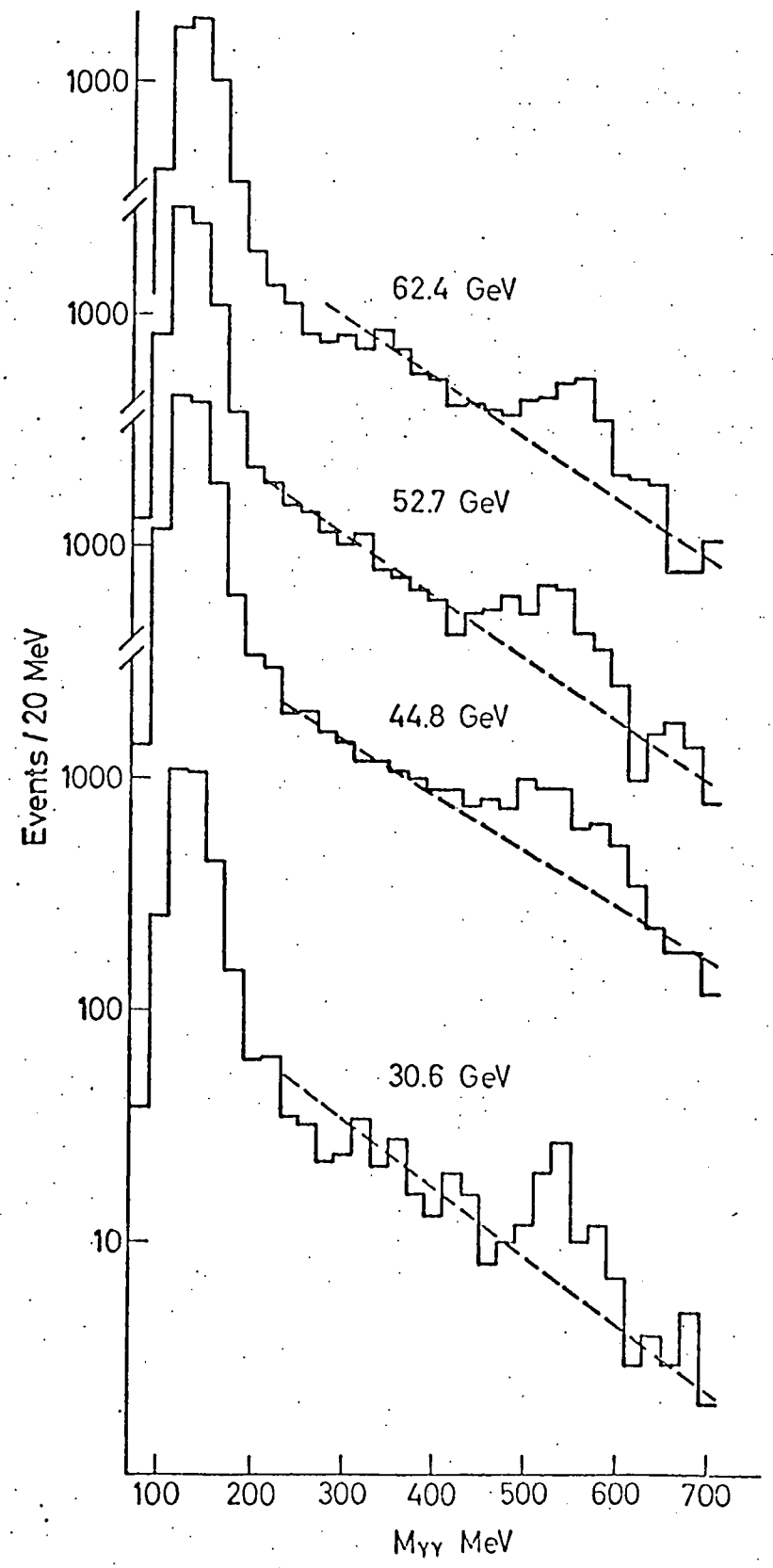
1000
1000
1000
1000
100
10
62.4 GeV
52.7 GeV
44.8 GeV
30.6 GeV
Events / 20 MeV
100
200
300
400
500
600
700
$M_{\gamma\gamma}$ MeV

Fig. 2

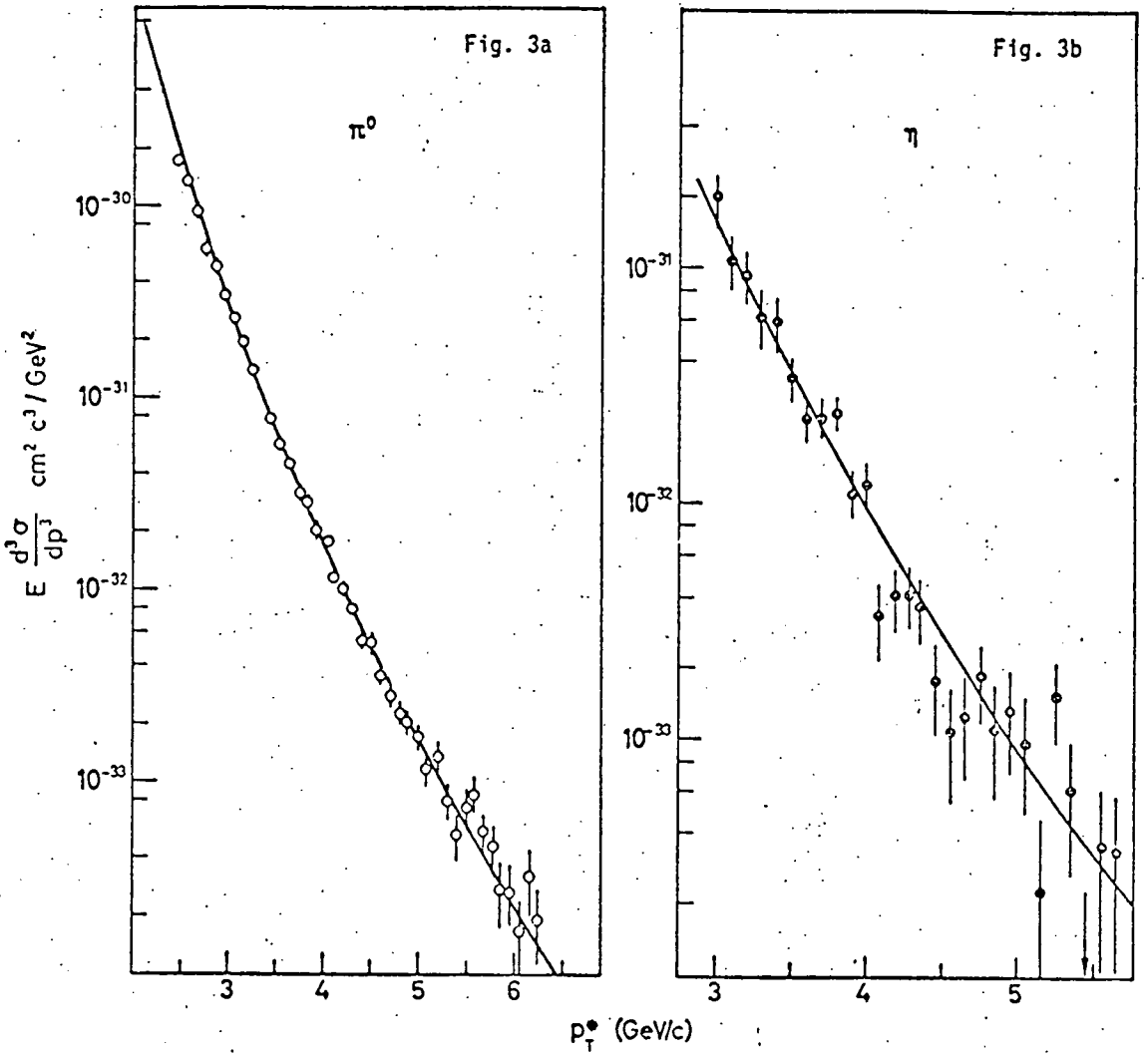
Fig. 3a
π^0
Fig. 3b
η
$E\frac{d^3\sigma}{dp^3}$ cm² c³ / GeV²
10^{-30}
10^{-31}
10^{-32}
10^{-33}
3
4
5
6
p_T^* (GeV/c)

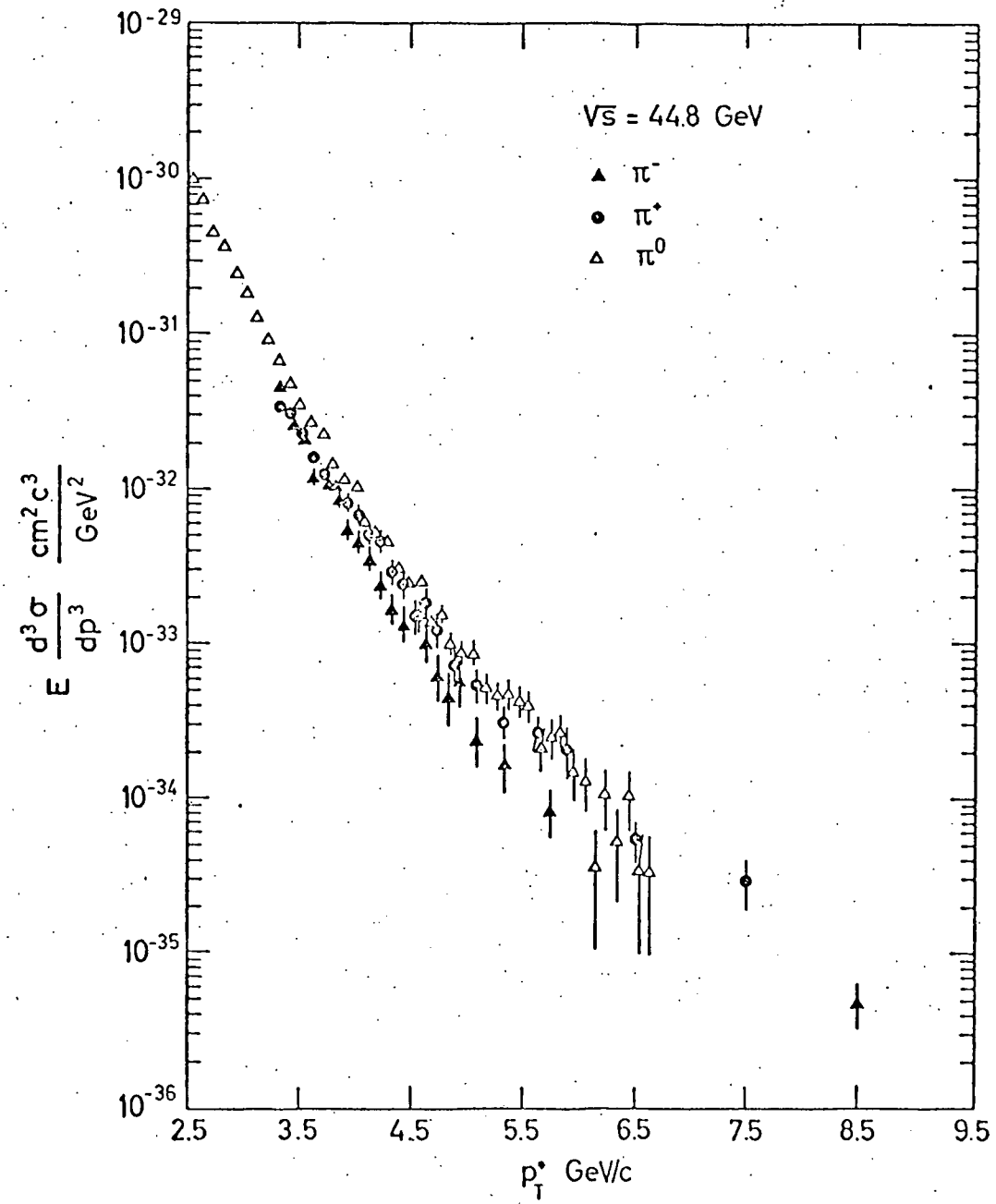
$\sqrt{s}$ = 44.8 GeV
π^-
π^+
π^0
$E\frac{d^3\sigma}{dp^3}\frac{cm^2c^3}{GeV^2}$
10^{-29}
10^{-30}
10^{-31}
10^{-32}
10^{-33}
10^{-34}
10^{-35}
10^{-36}
2.5
3.5
4.5
5.5
6.5
7.5
8.5
9.5
p_T^* GeV/c

Fig. 4a

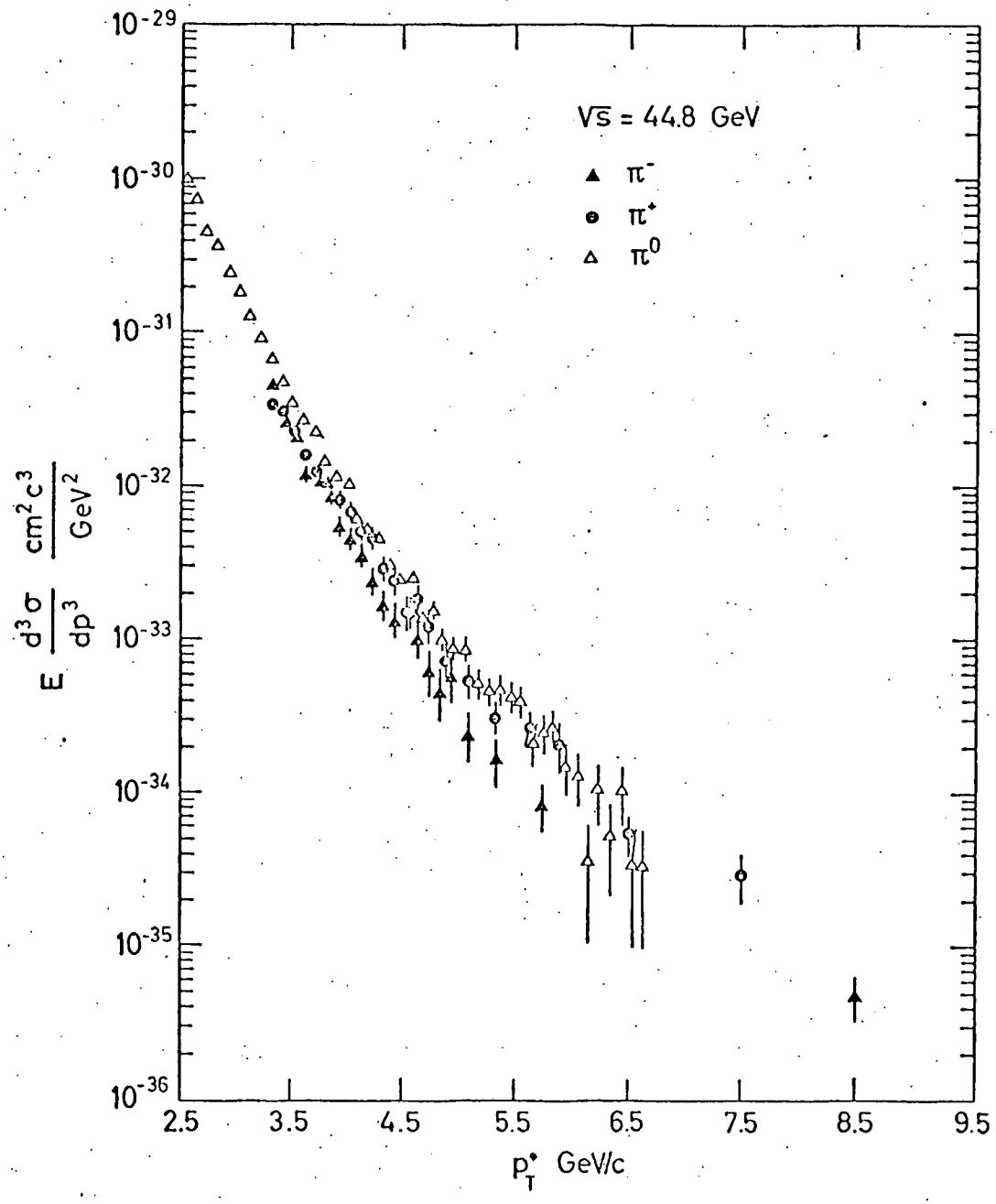
10^{-29}
10^{-30}
10^{-31}
10^{-32}
10^{-33}
10^{-34}
10^{-35}
10^{-36}
$E\frac{d^3\sigma}{dp^3}\frac{cm^2c^3}{GeV^2}$
$\sqrt{s}$ = 44.8 GeV
π^-
π^+
π^0
2.5
3.5
4.5
5.5
6.5
7.5
8.5
9.5
p_T^* GeV/c

Fig. 4b

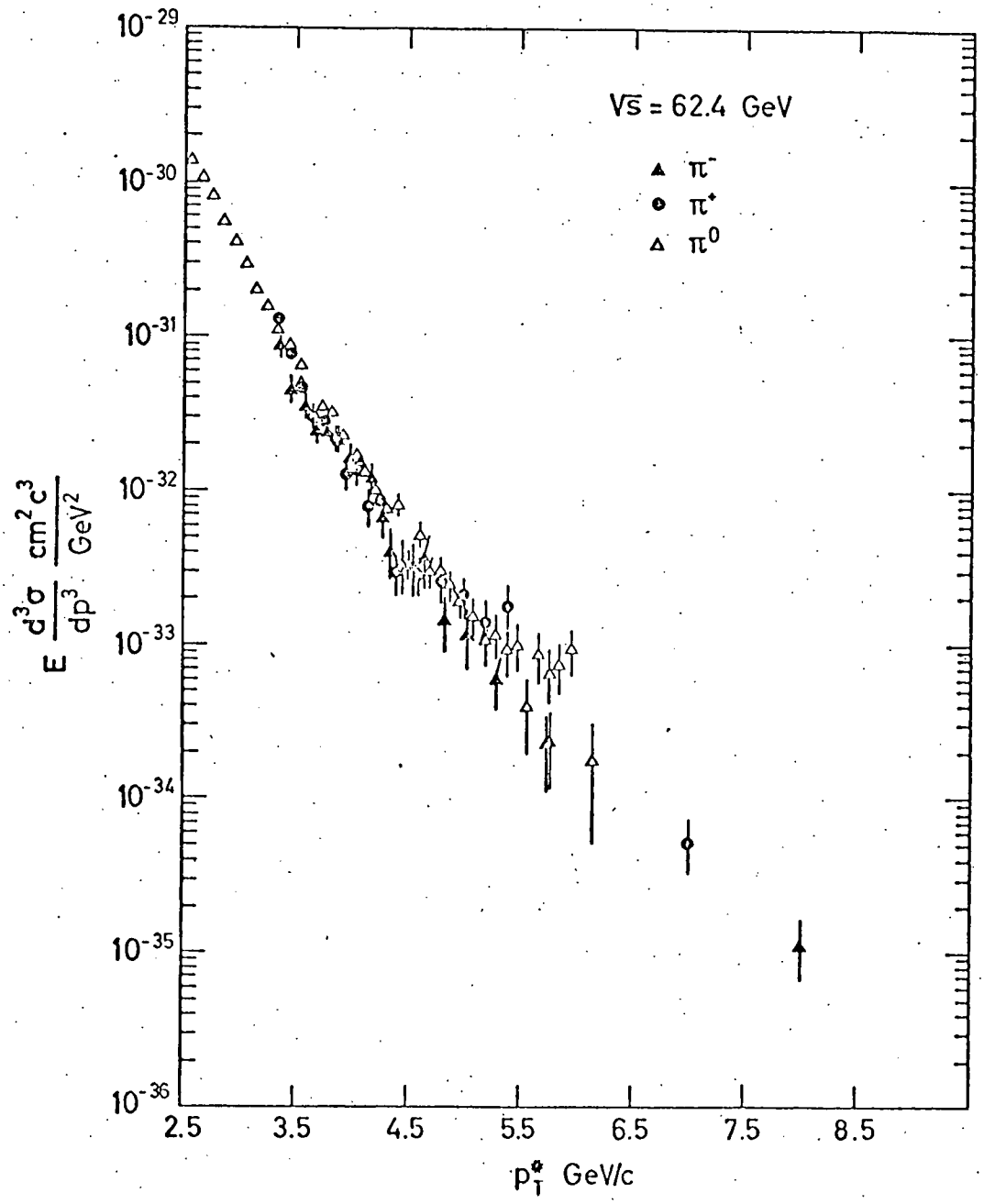
10^{-29}
10^{-30}
10^{-31}
10^{-32}
10^{-33}
10^{-34}
10^{-35}
10^{-36}
$E\frac{d^3\sigma}{dp^3}\frac{cm^2c^3}{GeV^2}$
$\sqrt{s}$ = 62.4 GeV
π^-
π^+
π^0
2.5
3.5
4.5
5.5
6.5
7.5
8.5
p_T^* GeV/c

Fig. 4c

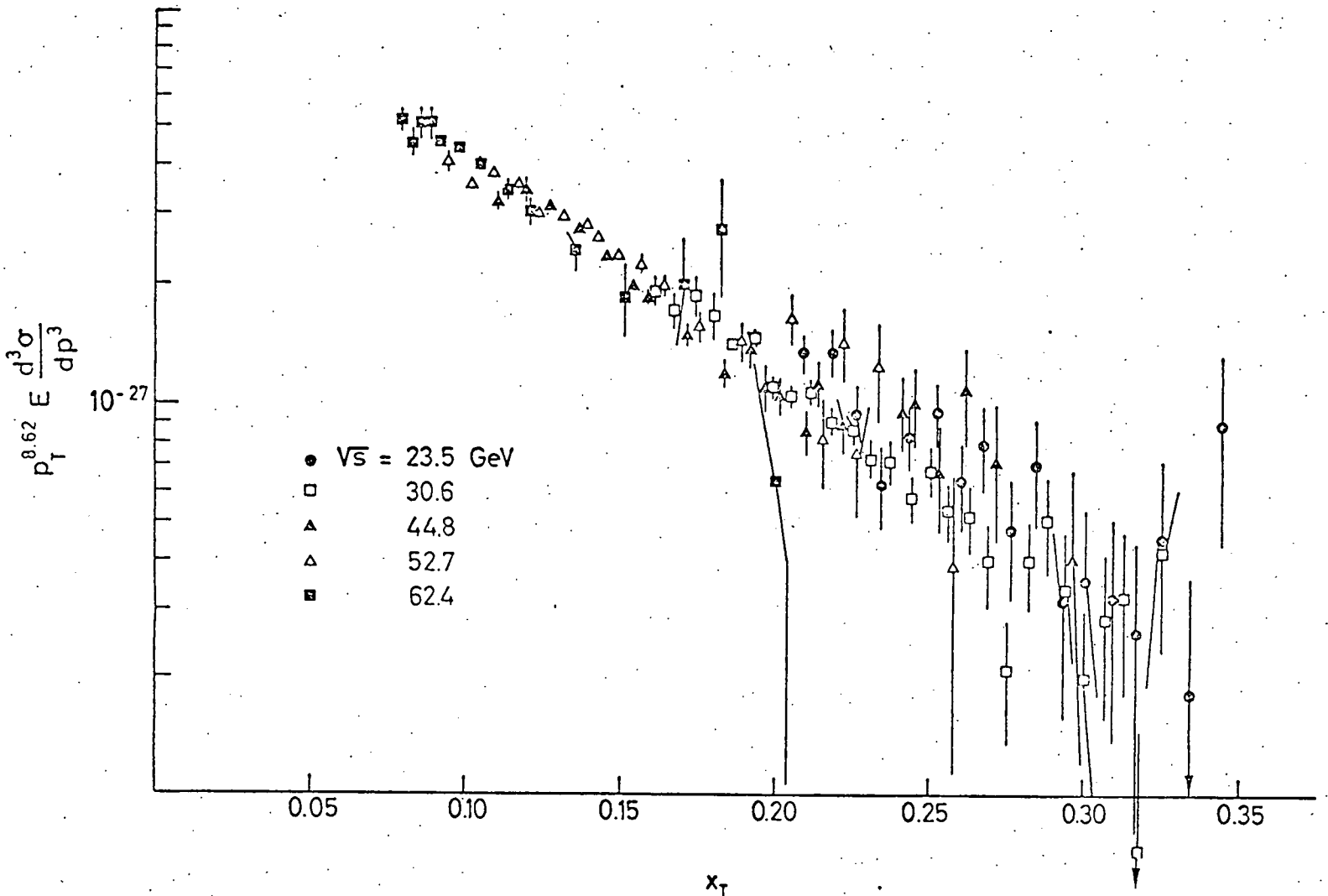
$p_T^{8.62} E \frac{d^3\sigma}{dp^3}$
10^{-27}
$\sqrt{s}$ = 23.5 GeV
30.6
44.8
52.7
62.4
0.05
0.10
0.15
0.20
0.25
0.30
0.35
x_T

Fig. 5

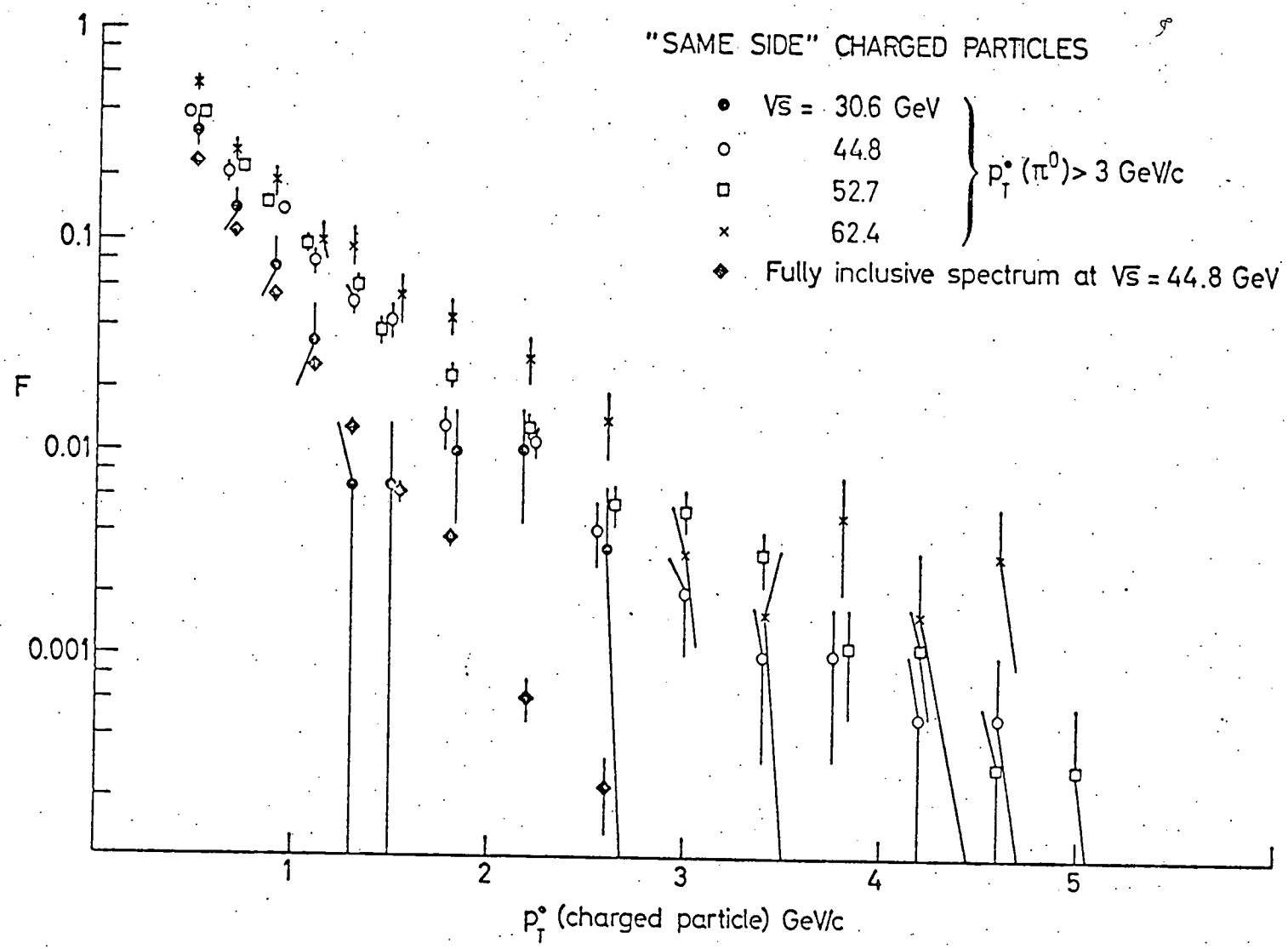
"SAME SIDE" CHARGED PARTICLES
√s = 30.6 GeV
44.8
52.7
62.4
p_T^* (π^0) > 3 GeV/c
Fully inclusive spectrum at √s = 44.8 GeV
F
1
0.1
0.01
0.001
1
2
3
4
5
p_T^* (charged particle) GeV/c

Fig. 6

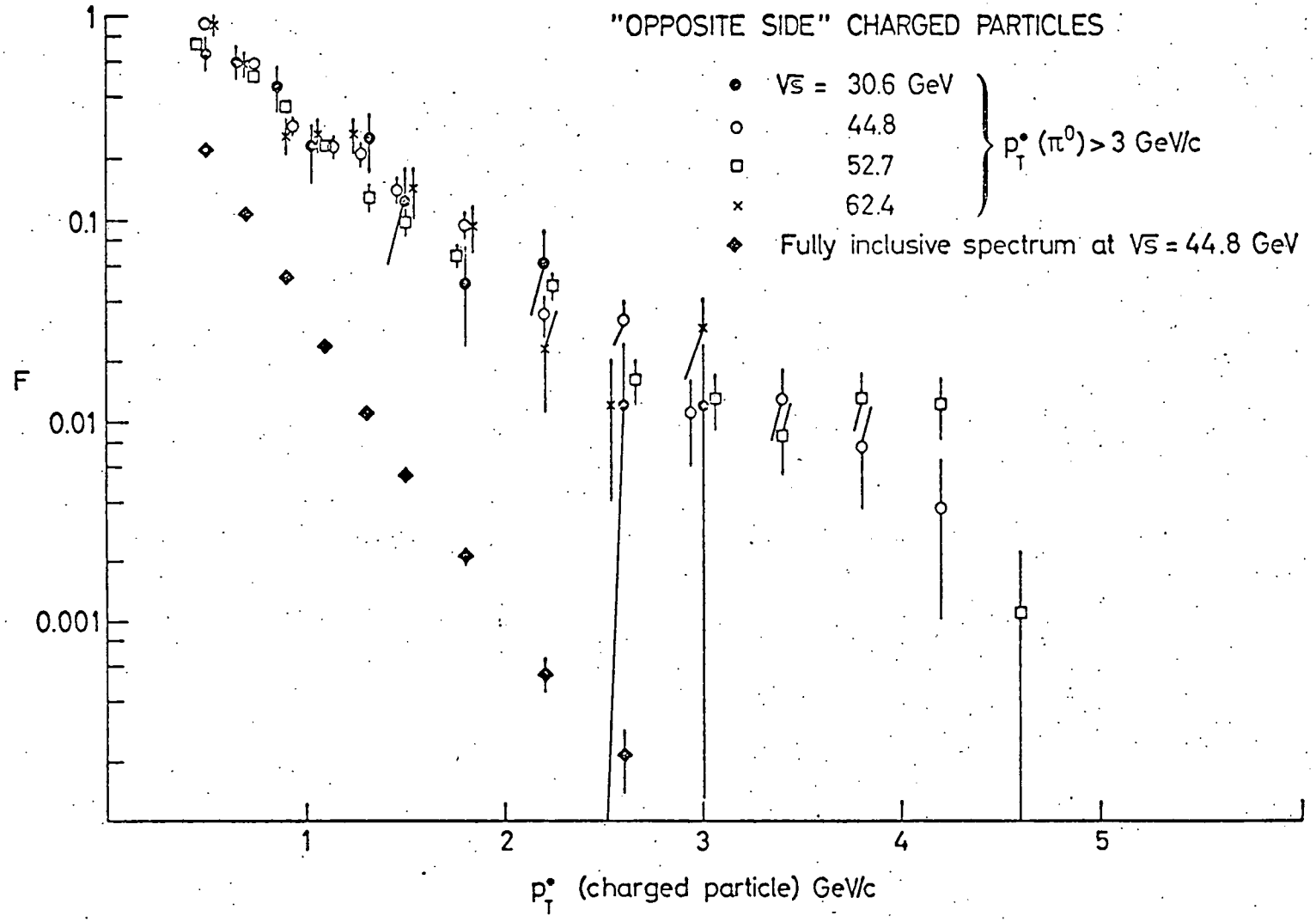
"OPPOSITE SIDE" CHARGED PARTICLES
√s = 30.6 GeV
44.8
52.7
62.4
p*T (π0) > 3 GeV/c
Fully inclusive spectrum at √s = 44.8 GeV
F
1
0.1
0.01
0.001
1
2
3
4
5
p*T (charged particle) GeV/c

Fig. 7

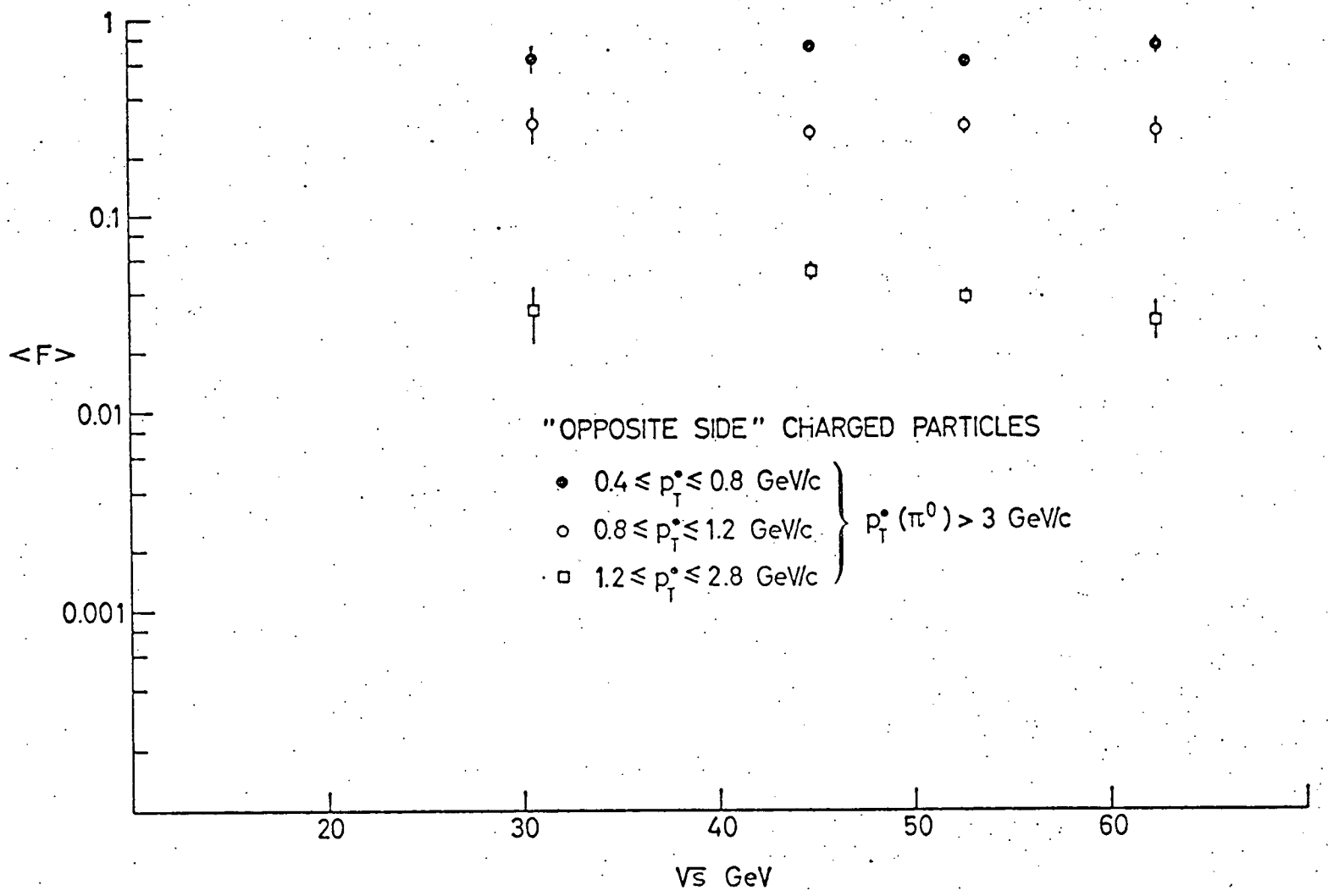
1
0.1
0.01
0.001
<F>
"OPPOSITE SIDE" CHARGED PARTICLES
0.4 ≤ p*T ≤ 0.8 GeV/c
0.8 ≤ p*T ≤ 1.2 GeV/c
1.2 ≤ p*T ≤ 2.8 GeV/c
p*T (π0) > 3 GeV/c
20
30
40
50
60
√s GeV

Fig. 8

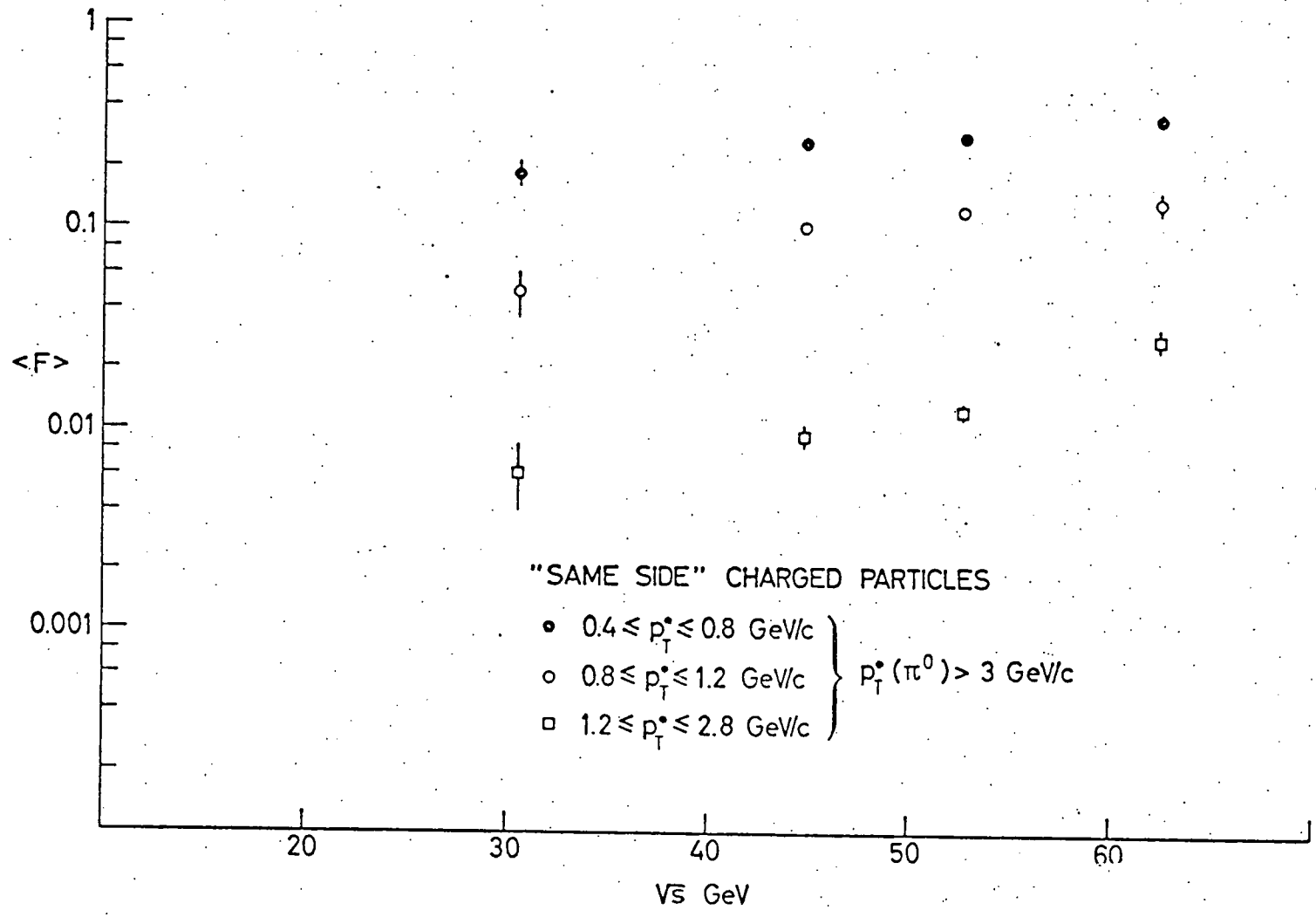
1
0.1
0.01
0.001
<F>
"SAME SIDE" CHARGED PARTICLES
0.4 ≤ p*T ≤ 0.8 GeV/c
0.8 ≤ p*T ≤ 1.2 GeV/c
1.2 ≤ p*T ≤ 2.8 GeV/c
p*T (π0) > 3 GeV/c
20
30
40
50
60
√s GeV

Fig. 9

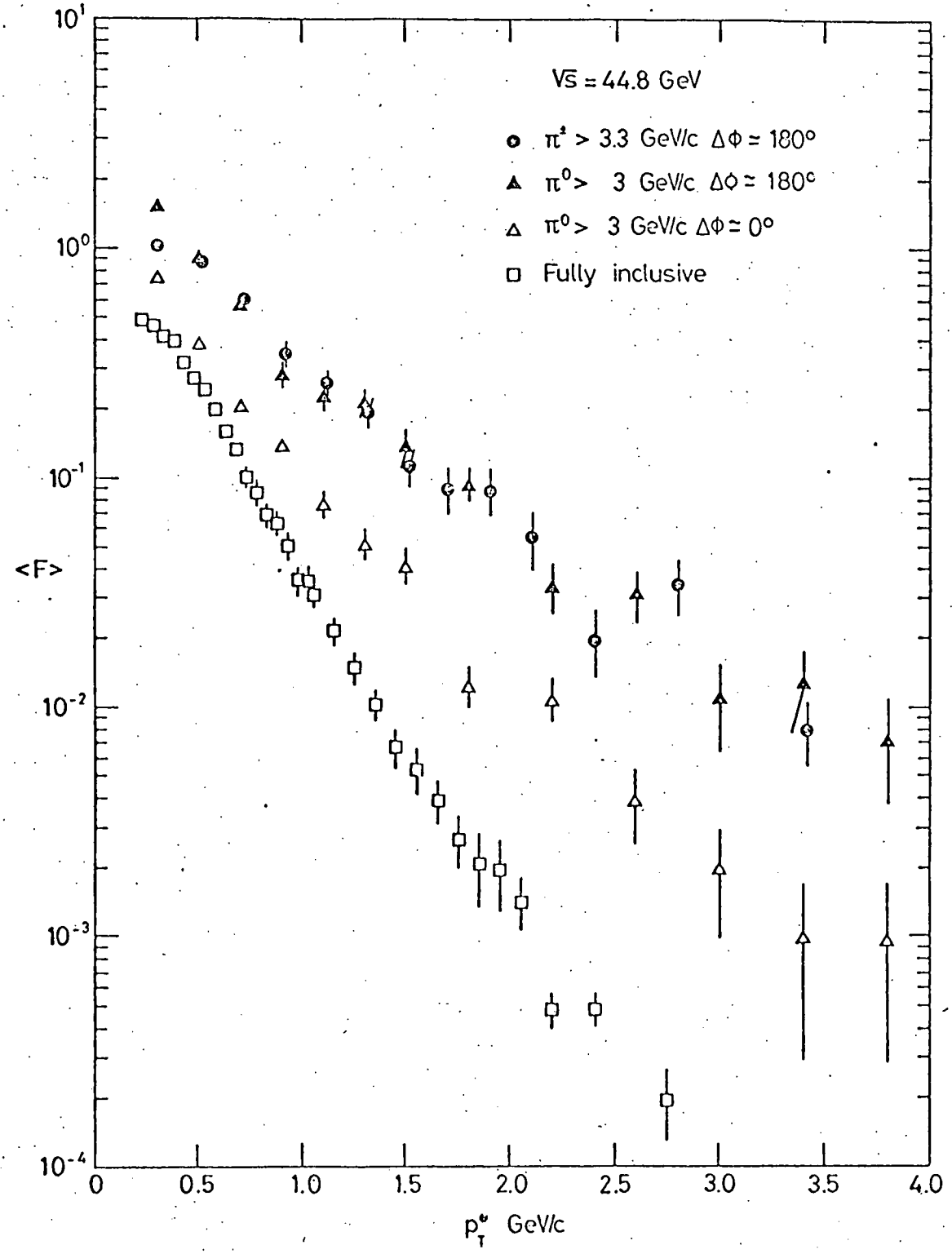
$\sqrt{s}$ = 44.8 GeV
$\pi^{\pm}$ > 3.3 GeV/c $\Delta\phi \simeq 180°$
π^0> 3 GeV/c $\Delta\phi \simeq 180°$
π^0> 3 GeV/c $\Delta\phi \simeq 0°$
Fully inclusive
<F>
p_T^{ψ} GeV/c

Fig. 10a

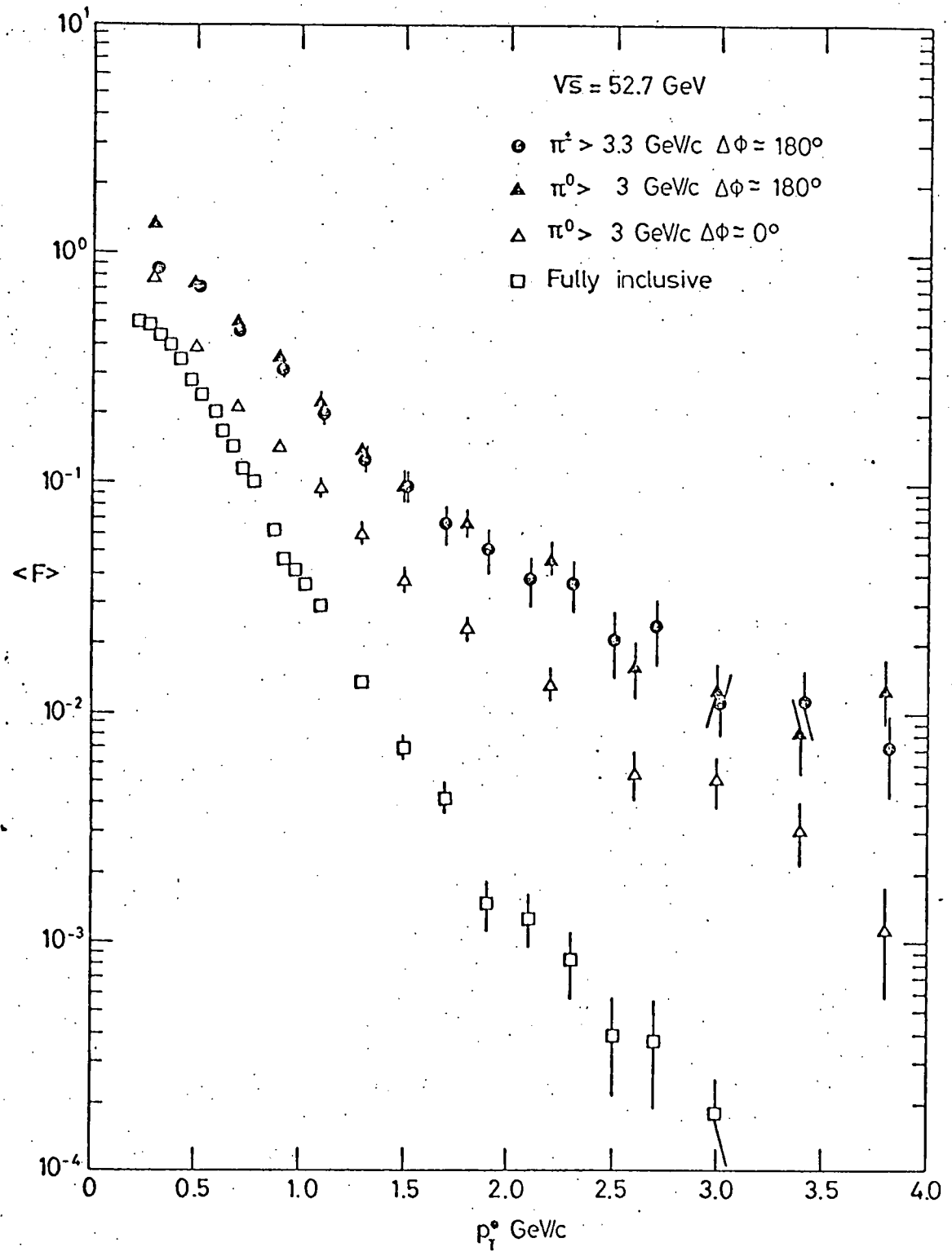
$\sqrt{s}$ = 52.7 GeV
$\pi^{\pm}$ > 3.3 GeV/c $\Delta\phi \simeq 180°$
π^0> 3 GeV/c $\Delta\phi \simeq 180°$
π^0> 3 GeV/c $\Delta\phi \simeq 0°$
Fully inclusive
<F>
p_T^* GeV/c

Fig. 10b

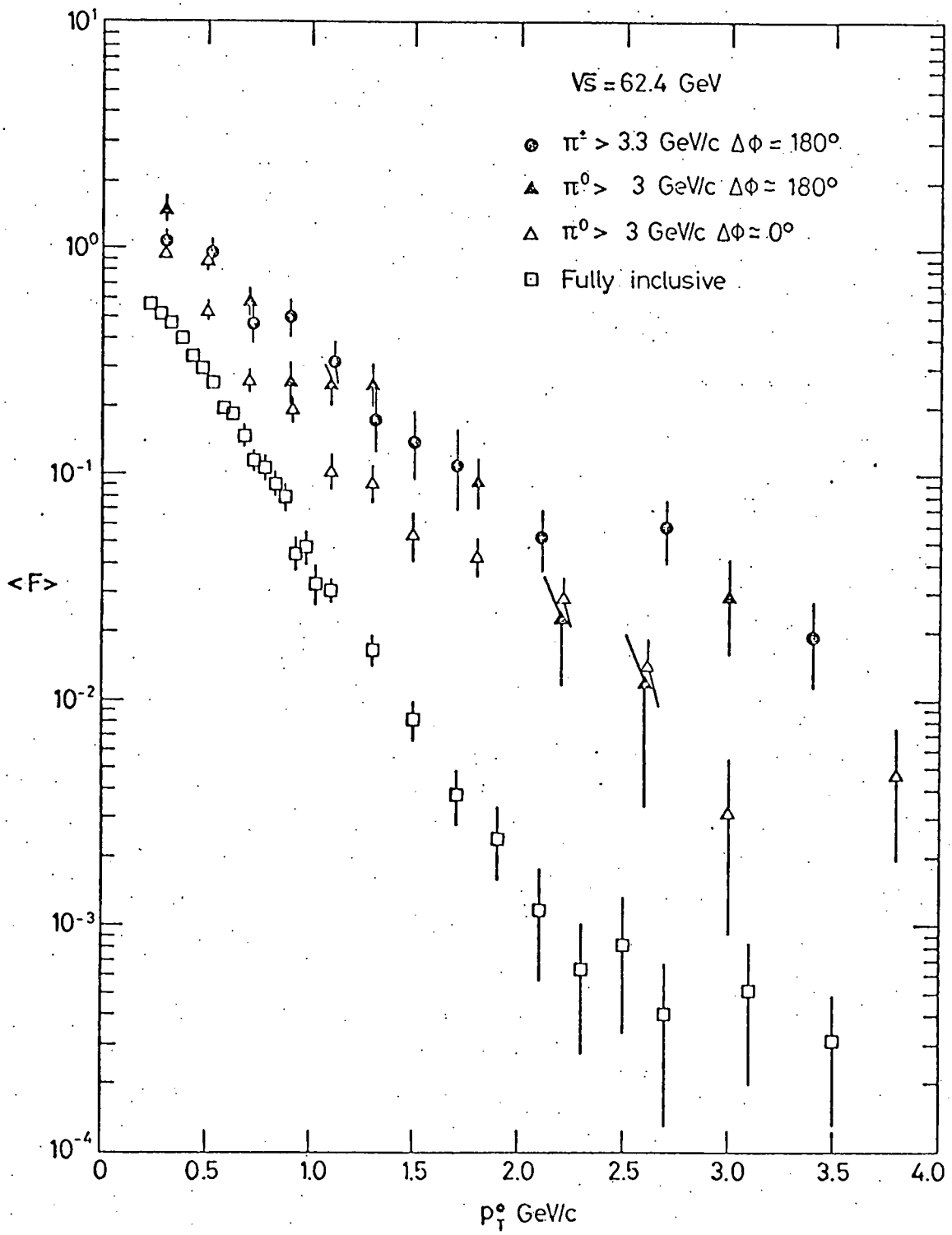
√s = 62.4 GeV
π± > 3.3 GeV/c Δφ = 180°
π⁰ > 3 GeV/c Δφ ≃ 180°
π⁰ > 3 GeV/c Δφ ≃ 0°
Fully inclusive
<F>
p_T GeV/c
10¹
10⁰
10⁻¹
10⁻²
10⁻³
10⁻⁴
0
0.5
1.0
1.5
2.0
2.5
3.0
3.5
4.0

Fig. 10c

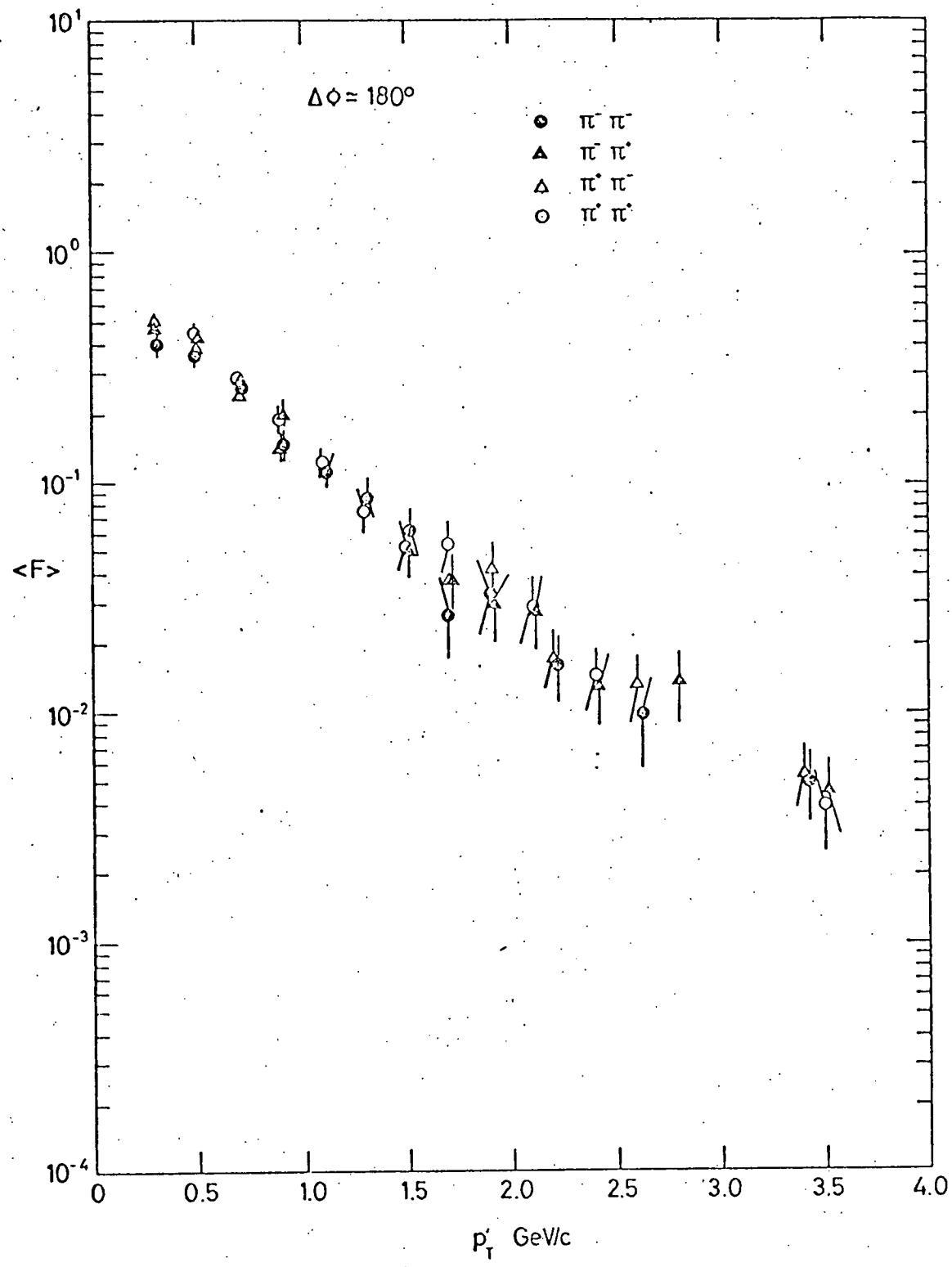
10^1
10^0
10^{-1}
10^{-2}
10^{-3}
10^{-4}
<F>
$\Delta\phi = 180°$
$\pi^- \pi^-$
$\pi^- \pi^+$
$\pi^+ \pi^-$
$\pi^+ \pi^+$
0
0.5
1.0
1.5
2.0
2.5
3.0
3.5
4.0
p_T' GeV/c

Fig. 11

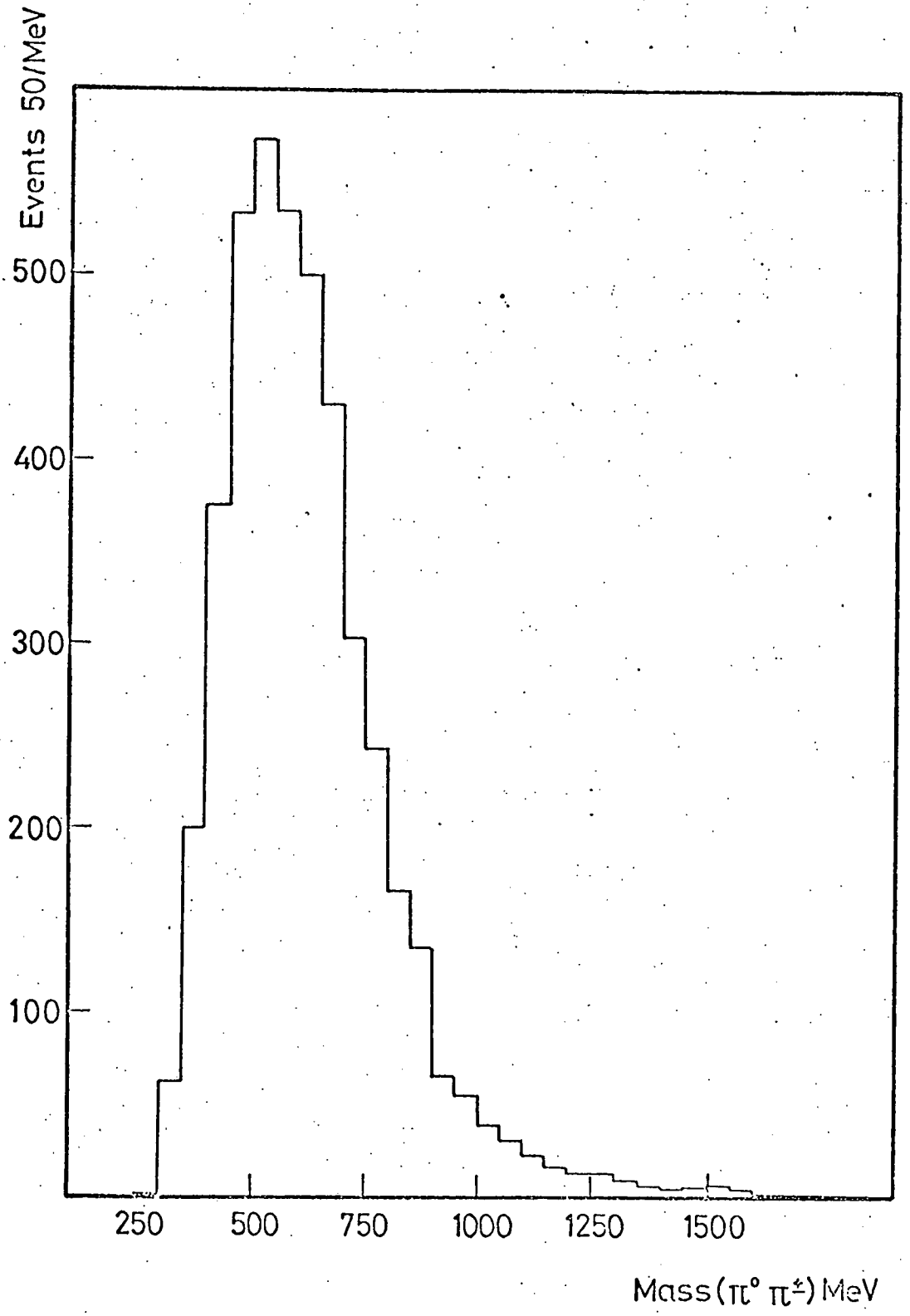
Events 50/MeV
500
400
300
200
100
250
500
750
1000
1250
1500
Mass (π° π±) MeV

Fig. 12